Volume 2 | Number 11 | 21 March 2014 | Pages 3679–4068

Journal of Materials Chemistry A

Materials for energy and sustainability

www.rsc.org/MaterialsA

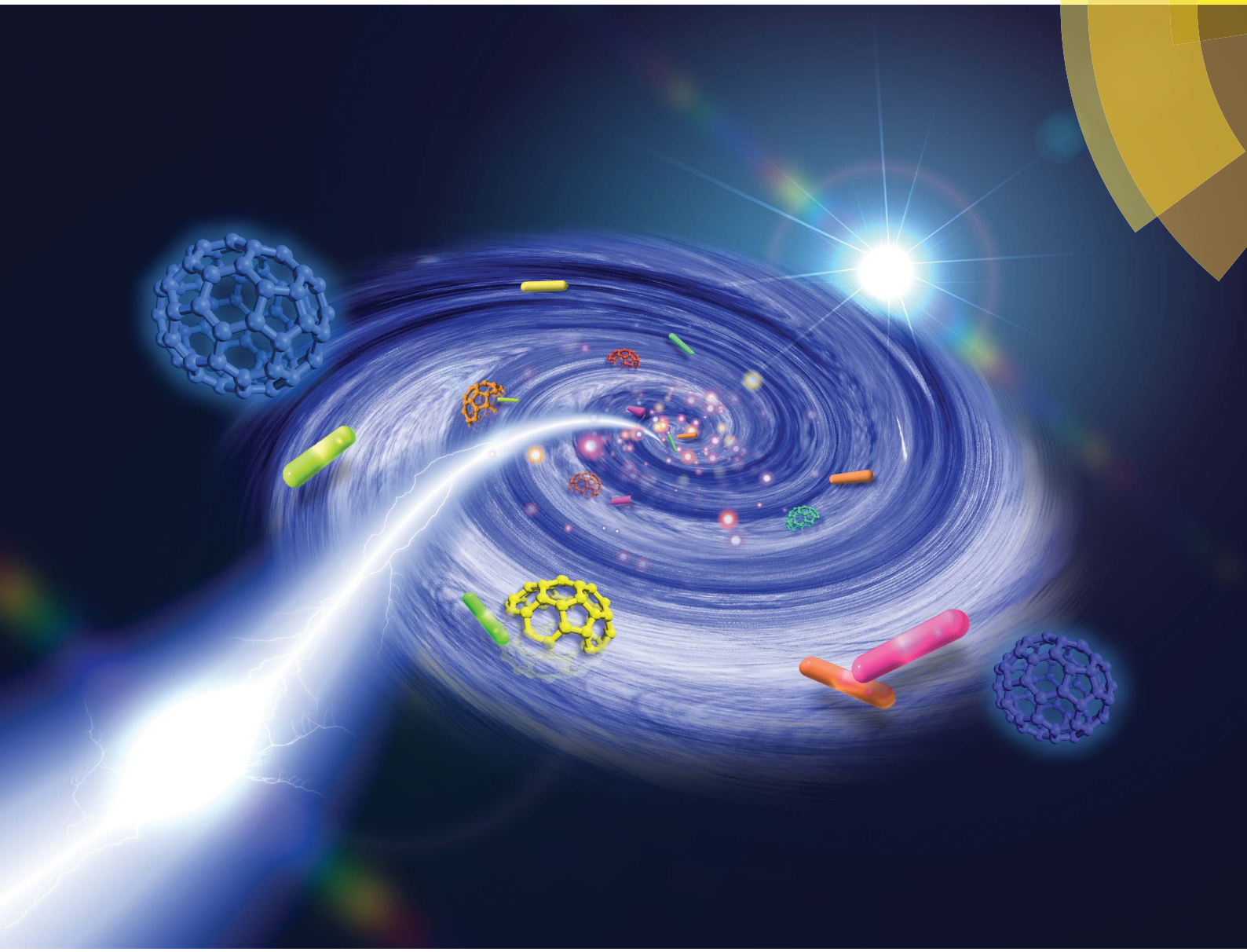

ISSN 2050-7488

ROYAL SOCIETY OF CHEMISTRY

COMMUNICATION

Hao-Wu Lin, Ken-Tsung Wong *et al.*

Highly efficient organic solar cells using a solution-processed active layer with a small molecule donor and pristine fullerene

Journal of Materials Chemistry A

COMMUNICATION

View Article Online
View Journal | View Issue

Cite this: J. Mater. Chem. A, 2014, 2, 3709

Received 11th December 2013
Accepted 7th January 2014

DOI: 10.1039/c3ta15138g

www.rsc.org/MaterialsA

Highly efficient organic solar cells using a solution-processed active layer with a small molecule donor and pristine fullerene†

Hao-Wu Lin,*[a] Jung-Hao Chang,[a] Wei-Ching Huang,[a] Yu-Ting Lin,[a] Li-Yen Lin,[b] Francis Lin,[b] Ken-Tsung Wong,*[bc] Hsiao-Fang Wang,[d] Rong-Ming Ho[d] and Hsin-Fei Meng[e]

A new strategy has been successfully established to realize high efficiency small molecule organic solar cells with a solution-processed active layer composed of a small organic molecule as the donor and pristine C_{70} as the acceptor. Using 1,2-dichlorobenzene as solvent, a homogeneous donor/C_{70} blend active layer can be effectively formed either by spin- or bar-coating techniques. This method delivers organic solar cells with high power conversion efficiencies up to 5.9%.

Introduction

Organic solar cells (OSCs) are emerging as a clean and competitive renewable energy resource due to their unique features including low-cost manufacturing, light weight, and mechanical flexibility. Among all OSCs, solution-processed organic bulk heterojunction (BHJ) solar cells, which consist of a phase-separated blend of a conjugated polymer as the electron donor and a fullerene derivative as the electron acceptor, have gained tremendous success.[1–11] Nevertheless, solution-processed OSCs utilizing small molecules as electron donors and acceptors received relatively less attention prior to 2006, but have gained growing attention recently.[12–19] Molecular donors offer facile solution-processing capability associated with polymers, and present specific advantages such as structural definition, easy synthesis and purification. Recently, solution-processed small molecule organic solar cells (SMOSCs) with power conversion efficiency (PCE) exceeding 8% have been successfully demonstrated.[19–21] To increase the solubility in solvent or to mimic the morphology control strategies developed for polymer-based solar cells, small molecule donors and acceptors suitable for the solution process were typically modified with long alkyl chains. However, the introduction of alkyl chains onto the conjugated backbone usually requires more synthetic steps which may raise the cost and energy in material production. Furthermore, long alkyl chains make these compounds hard to purify by sublimation, which is believed to be the best way of producing high purity materials for organic electronics. An alternative could be beneficial to achieve efficient solution-processed SMOSCs if the pristine donor and acceptor can be directly utilized without tedious synthesis and/or purification. This approach will potentially pave an effective way of producing low-cost light-harvesting devices. To this end, we have systematically investigated appropriate methods to fabricate bulk heterojunction composites of donors without long alkyl groups and pure C_{70}. For fair comparisons, the donors used in this report are molecules featuring a donor–acceptor–acceptor (D–A–A) configuration, which were previously utilized in vacuum-processed SMOSCs, where C_{70} was used as the acceptor. By carefully tuning the material compositions and solvents as well as deposition methods, solution-processed SMOSCs with high power efficiencies approaching to 6% have been successfully achieved. Our current results represent one major step forward in the development of cost-effective and low energy consumption SMOSCs.

Experimental

Device fabrication

Before thin film deposition, indium tin oxide (ITO) coated glass substrates (sheet resistance ~10 Ω sq^{-1}) were cleaned in an ultrasonic bath with de-ionized water, acetone, and methanol for 15 min, respectively. The MoO_3, CsF, Ca layers were deposited onto an ITO glass substrate in a high vacuum chamber with a base pressure of ~8×10^{-7} Torr, and the deposition was performed at a rate of 1–2 Å s^{-1} with the substrates held at room temperature.

[a]Department of Materials Science and Engineering, National Tsing Hua University, No. 101, Section 2, Kuang-Fu Road, Hsinchu, 30013, Taiwan. E-mail: hwlin@mx.nthu.edu.tw

[b]Department of Chemistry, National Taiwan University, No.1, Section 4, Roosevelt Road, Taipei, 10617, Taiwan. E-mail: kenwong@ntu.edu.tw

[c]Institute of Atomic and Molecular Sciences, Academia Sinica, No.1, Section 4, Roosevelt Road, Taipei, 10617, Taiwan. E-mail: kenwong@ntu.edu.tw

[d]Department of Chemical Engineering, National Tsing Hua University, Hsinchu, 30013, Taiwan

[e]Institute of Physics, National Chiao Tung University, Hsinchu, 30013, Taiwan

† Electronic supplementary information (ESI) available. See DOI: 10.1039/c3ta15138g

The sol–gel films of ZnO were spin-coated onto ITO glass substrates from a zinc acetate solution (7.3 mg mL^{-1}) in 96% 2-methoxy ethanol and 4% ethanolamine, and then annealed in air at 150 °C for 5 min. A blend solution of solar active donors and fullerene (purchased from Nano-C) was prepared using chloroform, chlorobenzene (CB), 1,2-dichlorobenzene (DCB) or 1,2,4-trichlorobenzene (TCB) as solvent with different ratios and a total concentration ranging from 12 to 30 mg mL^{-1}. The solution was stirred for 4 h at 65 °C, and cooled down to ambient temperature before casting. The active layers were spin-coated or bar-coated on a pre-treated substrate in a glove box under an anhydrous nitrogen atmosphere. For the spin-cast thin films, the layer thickness was controlled by the spin speed (800 to 3000 rpm) and solute concentration. For the bar-coated thin films, the layer thickness was controlled by the bar speed (60 to 450 mm s^{-1}) and solute concentration. The samples were then transferred to a vacuum chamber for sequential deposition of donor neat films, MoO_3, and a top Ag electrode. Devices were encapsulated using a UV-cured sealant (Everwide Chemical Co., Epowide EX) and a cover glass under an anhydrous nitrogen atmosphere after fabrication and were measured in air. The active area of the cells had an average size of 5 mm^2 (intersect area between the Ag cathode and the ITO anode) and were carefully measured device-by-device using a calibrated optical microscope. Thin films for TEM bright-field top-view investigation were prepared by immersing the glass/PEDOT:PSS/thin-film samples into deionized water. After dissolution of PEDOT:PSS, thin-films were floated onto the water surface and were transferred to a TEM grid.

Characterization measurements

Current density–voltage characteristics were measured with a Source Meter Keithley 2400 under AM 1.5G simulated solar illumination from a xenon lamp solar simulator (Abet Technologies). The incident light intensity was calibrated to be 100 mW cm^{-2} using a NREL-traceable KG5 filtered Si reference cell. The external quantum efficiency (EQE) spectra were taken by illuminating chopped monochromatic light with a continuous-wave bias white light (from a halogen lamp, intensity ~100 mW cm^{-2}) on the solar cells. The photocurrent signals were extracted by a lock-in technique using a current preamplifier (Stanford Research System) followed by a lock-in amplifier (AMETEK). The EQE measurement was fully computer controlled and the intensity of monochromatic light was carefully calibrated with a NIST-traceable optical power meter (Ophir Optronics). Thicknesses and extinction coefficients (k) of the thin films were determined using spectroscopic ellipsometry (J. A. Woollam Inc. V-VASE). Atomic force microscopy (AFM) images were analyzed with a Bruker Dimension Icon® Atomic Force Microscope operating in tapping mode. Transmission electron microscopy (TEM) images were analyzed with a JEOL JEM-1200X transmission electron microscope (accelerating voltage: 120 keV).

Results

Along the line of the conventional approach, hexyloxy groups were introduced onto a D–A–A donor (**DTDCTP**)[22,23] to give the modified donor **DP6DCTP** (Scheme 1) with improved solubility in organic solvents. In conjunction with the typical solution-processed acceptor [6,6]-phenyl-C_{61}-butyric acid methyl ester ($PC_{61}BM$), BHJ SMOSCs using **DP6DCTP**:$PC_{61}BM$ as the active layer were fabricated using a spin-casting technique. However, the achieved PCEs of 0.35–0.56% (see Fig. S1, ESI†) are far from satisfactory as compared to those of contemporary results.

The long alkyl groups in **DP6DCTP** are found to increase the solubility of the solution process. However, these non-conjugated hydrocarbons may increase the spatial occupation and thereby decrease the chromophore density in the active layer. Fortunately, we found that the parent donor **DTDCTP** showed good solubilities (>20 mg mL^{-1}) in various solvents such as chlorobenzene, 1,2-dichlorobenzene, and chloroform, which will be sufficient to form a strong absorbing layer with an adequate thickness (50–100 nm) for efficient light-harvesting. Encouraged by the high solubility of **DTDCTP**, SMOSCs with spin-coated **DTDCTP**:$PC_{61}BM$ (1 : 1) as the active layer configured into an inverted cell structure were fabricated. We adopted an inverted cell structure since it possesses several advantages such as the replacement of low T_g materials (ex: BCP) with hole-transporting metal oxide (ex: MoO_3) as the optical spacer between the active layer and metal electrodes[13,24,25] and/or the possibility to insert a donor neat film above the mixed active layer to facilitate hole-transport/extraction. One advantage of our donors is that they are able to form a homogeneous neat

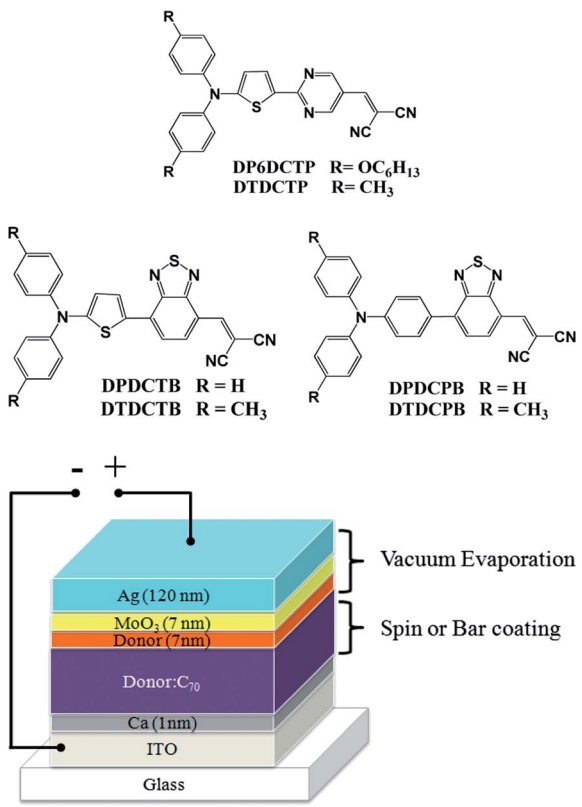

Scheme 1 Molecular structures of DP6DCTP, DTDCTP, DPDCPB, DTDCPB, DPDCTB, DTDCTB and the optimized device structure in this study.

film upon vacuum sublimation. Thus, a 7 nm donor neat film was introduced here, which can also increase a small portion of light absorption and thus contribute some photocurrent. Several modified transparent indium tin oxide (ITO) electrodes such as ITO (device A), ITO/sol–gel ZnO (device B), ITO/CsF (device C), and ITO/Ca (device D) were used as cathodes where MoO_3/Ag was used as the anode. The *J*–*V* characteristics and EQE spectra of devices A–D are shown in Fig. 1. Clearly, bare ITO without additional treatment (device A) shows the lowest PCE. In addition, the V_{oc} of device B was lowered down to 0.74 V, which was ascribed to high dark current owing to the high surface roughness ($R_{max} \sim 20$ nm measured by atomic force microscopy) of the sol–gel ZnO.[26,27] In contrast, devices C and D with ITO/CsF and ITO/Ca as cathodes show higher and comparable PCEs of 1.4 and 1.5%, respectively. As a result, ITO/Ca was selected as the cathode for our further studies. The inverted structure was configured as: ITO/Ca/mixed layer/donor layer/MoO_3/Ag (Scheme 1), where the mixed layer was formed by spin-coating, and then thin donor layer/MoO_3/Ag layers were vacuum deposited sequentially.

The acceptor $PC_{61}BM$ in device D was further replaced with [6,6]-phenyl-C_{71}-butyric acid methyl ester ($PC_{71}BM$), which exhibits similar electronic properties to $PC_{61}BM$, but shows a higher extinction coefficient (*k*) in the blue and cyan region (Fig. 2 inset). The effect of **DTDCTP**:$PC_{71}BM$ blend layer thickness (50–70 nm) on the device characteristics was further investigated (Fig. S2 in the ESI†). The best cell (device E) with a thin (50 nm) **DTDCTP**:$PC_{71}BM$ layer exhibits a J_{sc} of 7.46 mA cm^{-2}, a V_{oc} of 1.05 V, a FF of 30% and an overall PCE of 2.4% (Fig. 2). The thickness dependent device performances suggest that the bimolecular recombination becomes a dominant factor in these devices.

In spite of the solution processability of $PC_{61}BM$ and $PC_{71}BM$, pristine C_{70} exhibits the highest *k* in the visible spectrum region (Fig. 2 inset). As a consequence, C_{70} should be the best candidate to serve as the acceptor component to pair with **DTDCTP** with a feasible solution process for fabricating efficient SMOSCs, as we have achieved in vacuum-deposited devices.[22] However, this new idea is highly challenging due to the low solubility of C_{70} in common organic solvents and poor film-forming ability. Propitiously, we have found that DCB is able to dissolve adequate amounts of **DTDCTP** and C_{70} (greater than 20 mg mL^{-1}) for spin-casting. To our surprise, the efficiencies of spin-cast **DTDCTP**:C_{70} cells are largely enhanced. It is noteworthy that a trade-off between the increase of photon harvesting (thicker films) and the decrease of carrier recombination (thinner films) is found in the **DTDCTP**:C_{70} based devices with various thicknesses of the blend layer. This trade-off effect clearly results in a monotonic increase of J_{sc} values and decrease of FF values as the mixed layer thickness increases (see Fig. S3 in the ESI†). The optimized device (device F) with a **DTDCTP**:C_{70} (1 : 1.5) mixed layer thickness of *ca.* 50 nm shows an impressive PCE of 4.0% (Fig. 2), which is nearly 2 times that of the best **DTDCTP**:$PC_{71}BM$ cell. Obviously, this result indicates that efficient SMOSCs with solution-processed pristine C_{70} as the electron acceptor together with a small molecule as the electron donor can be easily achieved. The combination of a small molecule donor and pristine fullerene not only improves the cell performance but also provides a significant advantage of simplicity for molecular design and synthesis. To the best of our knowledge, our current method is new for giving efficient (PCE > 3%) solution-processed BHJ SMOSCs.

We believe that the performance enhancement should not be only limited to this specific case, but may generally apply to other small molecule systems. Along this line, a systematic study was conducted with this newly developed protocol using a series of D–A–A donors, namely, **DPDCPB**, **DTDCPB**, **DPDCTB**, and **DTDCTB** (Scheme 1). These small molecules were originally designed for vacuum-processed high efficiency SMOSCs.[28–31] The ratio of donor : C_{70} and the thickness of the spin-coated active layer have been carefully tuned (Fig. S4–S7, Tables S4–S7 in the ESI†). Fig. 3(a) shows the *J*–*V* characteristics of the optimized spin-cast devices and the data are summarized in Table 1. The optimized devices show high efficiencies up to 4.1% (device G: **DPDCPB**:C_{70}), 5.4% (device H: **DTDCPB**:C_{70}), 3.7% (device I: **DPDCTB**:C_{70}), and 5.2% (device J: **DTDCTB**:C_{70}).

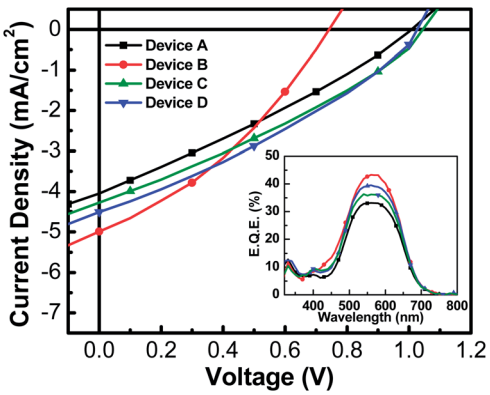

Fig. 1 *J*–*V* characteristics (under 1 sun, AM 1.5G illumination) and EQE spectra (inset) of the devices with the following structures: ITO/none (device A), sol–gel ZnO (device B), CsF (device C) and Ca (device D)/**DTDCTP**:$PC_{61}BM$ (1 : 1 by weight, 40 nm)/**DTDCTP** (7 nm)/MoO_3 (30 nm)/Ag (120 nm).

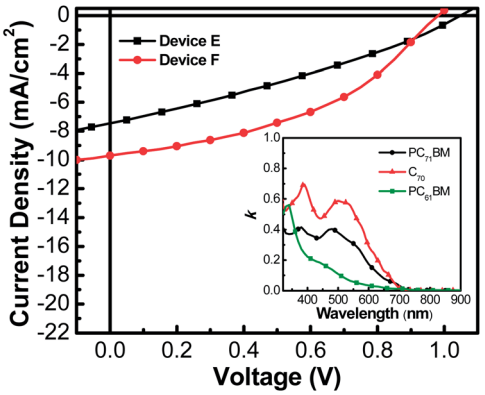

Fig. 2 *J*–*V* characteristics (under 1 sun, AM 1.5G illumination) of the devices with different acceptors. The device structures are ITO/Ca (1 nm)/**DTDCTP**:$PC_{71}BM$ (device E, 1 : 2 by weight, 50 nm) and **DTDCTP**:C_{70} (device F, 1 : 1.5 by weight, 50 nm)/**DTDCTP** (7 nm)/MoO_3 (7 nm)/Ag (120 nm), inset extinction coefficients of $PC_{71}BM$, C_{70} and $PC_{60}BM$.

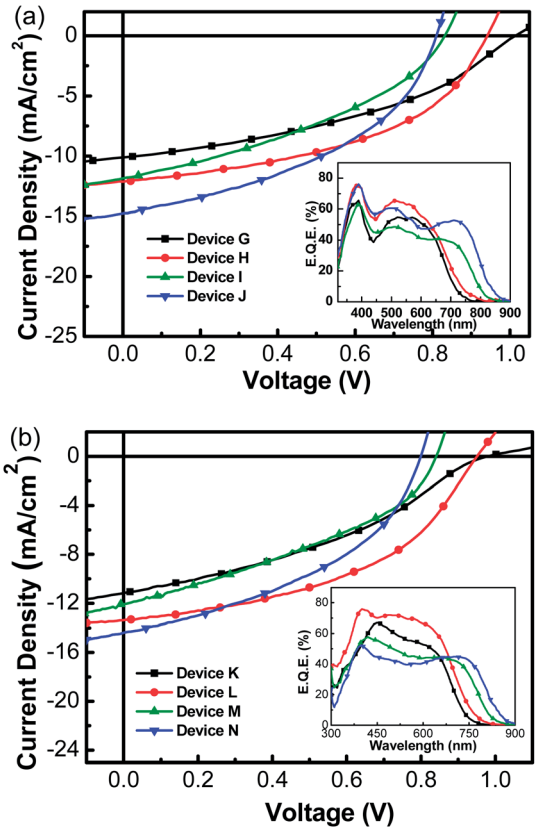

Fig. 3 *J–V* characteristics (under 1 sun, AM 1.5G illumination) and EQE spectra (inset) of solar cells fabricated from **DPDCPB** (devices G and K), **DTDCPB** (devices H and L), **DPDCTB** (devices I and M), and **DTDCTB** (devices J and N) by (a) spin-coating and (b) bar-coating processes. The device structures are: ITO/Ca (1 nm)/donor:C_{70}/donor (7 nm)/MoO_3 (7 nm)/Ag (120 nm).

In a well-optimized cell without carrier accumulation and interfacial recombination, the V_{oc} value of the device is usually correlated with the energy difference between the highest occupied molecular orbital (HOMO) level of the donors and the lowest unoccupied molecular orbital (LUMO) level of fullerene.[32] In this study, the differences in V_{oc} values of spin-cast cells are indeed related to the HOMO levels of donors as previously observed in vacuum-deposited ones.[29] On the other hand, the J_{sc} values depend on the bandgaps and extinction coefficients of these donors, which can be clearly verified in the EQE spectra. As shown in the inset of Fig. 3(a), the EQE spectra of both device I and device J exhibit broad responses covering the UV to near-infrared (IR) region. In particular, device J shows high EQE values of ~50% from the visible to near-IR wavelength range and extends the photoresponse up to 800 nm, resulting in a very high J_{sc} of 14.8 mA cm^{-2} and a PCE exceeding 5%. Moreover, through striking a balance between the photovoltage and photocurrent,[29] device H achieves the highest overall PCE of 5.4% with a V_{oc} of 0.94 V, a J_{sc} of 12.1 mA cm^{-2} and a FF of 47%. Compared to the vacuum-deposited cell in our previous reports,[22,28,29] the V_{oc} values of solution-processed devices are almost identical. However, the J_{sc} and FF values of spin-cast cells were ~10% lower, which is attributed to the simpler device structure (*i.e.* planar mixed heterojunction in vacuum-deposited devices *vs.* bulk heterojunction in spin-cast devices). As a result, the solution-processed devices achieve ~80% PCE of which the vacuum-deposited device counterparts can obtain. In addition, the FF values of these spin-cast devices range from 36 to 47%, which are on the low side of modern organic solar cells as compared to those utilizing polymers or tailor-made small molecules as electron donors. This could be ascribed to defective carrier transportation pathways[33] due to the lack of well-ordered D–A nanostructures, which were evidenced in the atomic force microscopy images of the spin-coated films (Fig. S8†). Nevertheless, our new results are quite promising in terms of simplicity and production costs.

In addition to the spin-coating method, a bar-coating technique was also adopted to fabricate an active layer for SMOSCs. The bar-coating technique has already been used in the fabrication of organic light emitting devices and polymer solar cells with favorable advantages such as better film formation and nearly 100% material utilization.[34,35] With DCB as solvent and the donor/acceptor ratio set to 1 : 2.2. These devices showed comparable PCEs to those of devices using the spin-cast technique (Fig. S9, Table S8 in the ESI†). One of the attractive benefits of solution-processed SMOSCs is the space for improving PCE by the manipulation of the active layer morphology. Among various treatments of the active layer for better PCEs, the *in situ* solvent-annealing has its merit of simplicity. Therefore, we adopted a co-solvent treatment for our bar-coated SMOSCs, allowing an extra ~20% improvement of performance in all benzothiadiazole-based D–A–A donor devices after the solvent composition optimization (see Fig. S10 and S11 and Tables S9 and S10 in the ESI†). The *J–V* characteristics of the optimized bar-coated devices are depicted in Fig. 3(b) and the data are summarized in Table 1, which are comparable to or even better than those of spin-cast devices in spite of obtaining similar bar-coated AFM images (Fig. S12†) of the active layers. However, a D–A segregation domain size of ~20 nm can be observed in the AFM phase images, which led to higher PCEs in **DTDCPB**- and **DTDCTB**-based devices as

Table 1 Performance parameters of the optimized devices under AM 1.5G simulated solar illumination at an intensity of 100 mW cm^{-2}

Device type	V_{oc} (V)	J_{sc} (mA cm^{-2})	FF (%)	η (%)
Device F: **DTDCTP**:C_{70} (1 : 1.5)[a]	0.98	9.7	42	4.0
Device G: **DPDCPB**:C_{70} (1 : 1.5)[a]	1.01	10.9	40	4.1
Device H: **DTDCPB**:C_{70} (1 : 1.5)[a]	0.94	12.1	47	5.4
Device I: **DPDCTB**:C_{70} (1 : 2.0)[a]	0.83	11.9	37	3.7
Device J: **DTDCTB**:C_{70} (1 : 1.8)[a]	0.81	14.8	43	5.2
Device K: **DPDCPB**:C_{70} (1 : 2.2)[b]	0.98	11.1	36	3.9
Device L: **DTDCPB**:C_{70} (1 : 2.2)[b]	0.95	13.4	46	5.9
Device M: **DPDCTB**:C_{70} (1 : 2.2)[c]	0.85	12.1	37	3.8
Device N: **DTDCTB**:C_{70} (1 : 2.2)[b]	0.82	14.5	43	5.1

[a] Active-layer thin films were cast from 1,2-dichlorobenzene solution by a spin-coating process. [b] Active-layer thin films were cast from 1,2-dichlorobenzene and 1,2,4-trichlorobenzene mixture solutions (1 : 1 by volume) by a bar-coating process. [c] Active-layer thin films were cast from 1,2-dichlorobenzene and chlorobenzene mixture solutions (7 : 3 by volume) by a bar-coating process.

compared to those of **DPDCPB**- and **DPDCTB**-based ones. The best bar-coated devices show PCEs of 3.9% (device K: **DPDCPB**:C_{70}), 5.9% (device L: **DTDCPB**:C_{70}), 3.8% (device M: **DPDCTB**:C_{70}) and 5.1% (device N: **DTDCTB**:C_{70}). Interestingly, the characteristics such as V_{oc},J_{sc} and EQE spectra of optimized devices show similar trends regardless of the different thin-film formation methods. Among them, the bar-coated devices employing **DTDCPB** as the electron donor combined with C_{70} as the acceptor (device L) show the best performance with a V_{oc} of 0.95, a J_{sc} of 13.4 mA cm^{-2}, a fill factor of 46% and a PCE as high as 5.9%. This result is consistent with our previous observations from the vacuum-processed and spin-cast SMOSCs. More importantly, ~90% efficiency of the vacuum-deposited cell (PCE = 6.8%) using the same donor and acceptor now can be achieved with this newly developed method.

Because the AFM results only provide information on surface morphology, we then further probed the bulk morphology by using TEM. Three samples were prepared: (a) **DTDCPB**:C_{70} (1 : 1.5) thin film spin-cast from a DCB solution, (b) **DTDCPB**:C_{70} (1 : 2.2) thin film bar-coated from a DCB solution, and (c) **DTDCPB**:C_{70} (1 : 2.2) thin film bar-coated from a DCB and TCB (1 : 1 by volume) mixed solution. These samples correspond to the most efficient devices (devices H, S_{21}, and L) obtained by spin-coating and bar-coating methods respectively. The results are shown in Fig. S13.† Both D–A blend films cast from a DCB solution by spin- and bar-coating processes exhibited a less distinctly resolved domain structure and larger features as compared to that of the thin film cast from a DCB/TCB mixed solution. The distinct domain and smaller domain size formation in the thin film cast from DCB/TCB mixed solution could assist both exciton separation and carrier transportation, leading to the highest device performance in this work.

Conclusions

In summary, a new strategy for the realization of SMOSCs with a solution-processed BHJ active layer composed of organic compounds without long alkyl substitutions as the donor and pristine C_{70} as the acceptor has been successfully established. The donor/C_{70} blend active layer can be effectively formed either by spin-coating or bar-coating techniques. This new method can be generally applied to various organic D–A–A donors, delivering SMOSCs with high PCEs up to 5.9%, which is about 90% of the best device fabricated by the vacuum deposition technique. We believe that the work accomplished in this paper can facilitate the development of new organic molecules as low-cost donor materials and provide new guidelines for the fabrication of highly efficient solution-processed organic photovoltaics.

Acknowledgements

We thank the National Science Council of Taiwan (NSC 101-2113-M-002-009-MY3, NSC-102-2221-E-007-125-MY3, NSC-101-2112-M-007-017-MY3), Academia Sinica (AS-103-SS-A02), and the Low Carbon Energy Research Center, National Tsing-Hua University, for financial support.

Notes and references

1 J. You, L. Dou, K. Yoshimura, T. Kato, K. Ohya, T. Moriarty, K. Emery, C. C. Chen, J. Gao, G. Li and Y. Yang, *Nat. Commun.*, 2013, **4**, 1446.
2 Z. Tan, W. Zhang, Z. Zhang, D. Qian, Y. Huang, J. Hou and Y. Li, *Adv. Mater.*, 2012, **24**, 1476.
3 M. S. Su, C. Y. Kuo, M. C. Yuan, U. S. Jeng, C. J. Su and K. H. Wei, *Adv. Mater.*, 2011, **23**, 3315.
4 C. Duan, F. Huang and Y. Cao, *J. Mater. Chem.*, 2012, **22**, 10416.
5 T. Y. Chu, J. Lu, S. Beaupre, Y. Zhang, J. R. Pouliot, S. Wakim, J. Zhou, M. Leclerc, Z. Li, J. Ding and Y. Tao, *J. Am. Chem. Soc.*, 2011, **133**, 4250.
6 Z. He, C. Zhong, X. Huang, W. Y. Wong, H. Wu, L. Chen, S. Su and Y. Cao, *Adv. Mater.*, 2011, **23**, 4636.
7 H. Zhou, L. Yang, A. C. Stuart, S. C. Price, S. Liu and W. You, *Angew. Chem., Int. Ed.*, 2011, **50**, 2995.
8 C. E. Small, S. Chen, J. Subbiah, C. M. Amb, S.-W. Tsang, T. H. Lai, J. R. Reynolds and F. So, *Nat. Photonics*, 2012, **6**, 115.
9 T. Yang, M. Wang, C. Duan, X. Hu, L. Huang, J. Peng, F. Huang and X. Gong, *Energy Environ. Sci.*, 2012, **5**, 8208.
10 J. M. Szarko, J. Guo, Y. Liang, B. Lee, B. S. Rolczynski, J. Strzalka, T. Xu, S. Loser, T. J. Marks, L. Yu and L. X. Chen, *Adv. Mater.*, 2010, **22**, 5468.
11 B. Walker, J. Liu, C. Kim, G. C. Welch, J. K. Park, J. Lin, P. Zalar, C. M. Proctor, J. H. Seo, G. C. Bazan and T.-Q. Nguyen, *Energy Environ. Sci.*, 2013, **6**, 952.
12 T. Bura, N. Leclerc, S. Fall, P. Leveque, T. Heiser, P. Retailleau, S. Rihn, A. Mirloup and R. Ziessel, *J. Am. Chem. Soc.*, 2012, **134**, 17404.
13 H. Y. Lin, W. C. Huang, Y. C. Chen, H. H. Chou, C. Y. Hsu, J. T. Lin and H. W. Lin, *Chem. Commun.*, 2012, **48**, 8913.
14 H. Tanaka, Y. Abe, Y. Matsuo, J. Kawai, I. Soga, Y. Sato and E. Nakamura, *Adv. Mater.*, 2012, **24**, 3521.
15 J. Huang, C. Zhan, X. Zhang, Y. Zhao, Z. Lu, H. Jia, B. Jiang, J. Ye, S. Zhang, A. Tang, Y. Liu, Q. Pei and J. Yao, *ACS Appl. Mater. Interfaces*, 2013, **5**, 2033.
16 T. S. van der Poll, J. A. Love, T. Q. Nguyen and G. C. Bazan, *Adv. Mater.*, 2012, **24**, 3646.
17 X. Xiao, G. Wei, S. Wang, J. D. Zimmerman, C. K. Renshaw, M. E. Thompson and S. R. Forrest, *Adv. Mater.*, 2012, **24**, 1956.
18 A. K. Kyaw, D. H. Wang, V. Gupta, J. Zhang, S. Chand, G. C. Bazan and A. J. Heeger, *Adv. Mater.*, 2013, **25**, 2397.
19 J. J. Jasieniak, B. B. Y. Hsu, C. J. Takacs, G. C. Welch, G. C. Bazan, D. Moses and A. J. Heeger, *ACS Nano*, 2012, **6**, 8735.
20 J. Zhou, Y. Zuo, X. Wan, G. Long, Q. Zhang, W. Ni, Y. Liu, Z. Li, G. He, C. Li, B. Kan, M. Li and Y. Chen, *J. Am. Chem. Soc.*, 2013, **135**, 8484.
21 V. Gupta, A. K. K. Kyaw, D. H. Wang, S. Chand, G. C. Bazan and A. J. Heeger, *Sci. Rep.*, 2013, **3**, 1965.

22 S. W. Chiu, L. Y. Lin, H. W. Lin, Y. H. Chen, Z. Y. Huang, Y. T. Lin, F. Lin, Y. H. Liu and K. T. Wong, *Chem. Commun.*, 2012, **48**, 1857.
23 H. W. Lin, S. W. Chiu, L. Y. Lin, Z. Y. Hung, Y. H. Chen, F. Lin and K. T. Wong, *Adv. Mater.*, 2012, **24**, 2269.
24 D. W. Zhao, P. Liu, X. W. Sun, S. T. Tan, L. Ke and A. K. K. Kyaw, *Appl. Phys. Lett.*, 2009, **95**, 153304.
25 C. Y. Jiang, X. W. Sun, D. W. Zhao, A. K. K. Kyaw and Y. N. Li, *Sol. Energy Mater. Sol. Cells*, 2010, **94**, 1618.
26 Z. Ma, Z. Tang, E. Wang, M. R. Andersson, O. Inganäs and F. Zhang, *J. Phys. Chem. C*, 2012, **116**, 24462.
27 C. Trinh, J. R. Bakke, T. P. Brennan, S. F. Bent, F. Navarro, A. Bartynski and M. E. Thompson, *Appl. Phys. Lett.*, 2012, **101**, 233903.
28 L. Y. Lin, Y. H. Chen, Z. Y. Huang, H. W. Lin, S. H. Chou, F. Lin, C. W. Chen, Y. H. Liu and K. T. Wong, *J. Am. Chem. Soc.*, 2011, **133**, 15822.
29 Y. H. Chen, L. Y. Lin, C. W. Lu, F. Lin, Z. Y. Huang, H. W. Lin, P. H. Wang, Y. H. Liu, K. T. Wong, J. Wen, D. J. Miller and S. B. Darling, *J. Am. Chem. Soc.*, 2012, **134**, 13616.
30 H.-W. Lin, H.-W. Kang, Z.-Y. Huang, C.-W. Chen, Y.-H. Chen, L.-Y. Lin, F. Lin and K.-T. Wong, *Org. Electron.*, 2012, **13**, 1925.
31 H.-W. Lin, C.-W. Lu, L.-Y. Lin, Y.-H. Chen, W.-C. Lin, K.-T. Wong and F. Lin, *J. Mater. Chem. A*, 2013, **1**, 1770.
32 M. C. Scharber, D. Mühlbacher, M. Koppe, P. Denk, C. Waldauf, A. J. Heeger and C. J. Brabec, *Adv. Mater.*, 2006, **18**, 789.
33 Y. Zhang, X.-D. Dang, C. Kim and T.-Q. Nguyen, *Adv. Energy Mater.*, 2011, **1**, 610.
34 H.-C. Yeh, H.-F. Meng, H.-W. Lin, T.-C. Chao, M.-R. Tseng and H.-W. Zan, *Org. Electron.*, 2012, **13**, 914.
35 J.-H. Chang, Y.-H. Chen, H.-W. Lin, Y.-T. Lin, H.-F. Meng and E.-C. Chen, *Org. Electron.*, 2012, **13**, 705.

